Available online at www.sciencedirect.com
ScienceDirect
Journal of Sound and Vibration 301 (2007) 59–73
JOURNAL OF SOUND AND VIBRATION
www.elsevier.com/locate/jsvi

Numerical and experimental investigations of the nonlinear dynamics and chaos in non-smooth systems

Marcelo Amorim Savi[a,*], Sandor Divenyi[a], Luiz Fernando Penna Franca[b], Hans Ingo Weber[c]

[a]*Department of Mechanical Engineering, Universidade Federal do Rio de Janeiro, COPPE, P.O. Box 68.503 21.941.972, Rio de Janeiro, RJ, Brazil*
[b]*CSIRO Petroleum—Drilling Mechanics, P.O. Box 1130, Bentley WA 6102, Kensington, WA 6151, Australia*
[c]*Department of Mechanical Engineering, Pontifícia Universidade Católica do Rio de Janeiro 22.453.900, Rio de Janeiro, RJ, Brazil*

Received 24 June 2005; received in revised form 4 August 2006; accepted 5 September 2006
Available online 1 November 2006

Abstract

Nature is full of non-smooth nonlinearities that are usually related to either friction phenomena or the discontinuous characteristics of intermittent contacts. In general, non-smooth characteristics cause difficulties in the modeling and simulation of natural systems. A smoothed switch model is used in this contribution in order to analyze non-smooth systems. The procedure is shown to be an effective method of dealing with this kind of system, and has advantages in numerical implementation. As an application of the general formulation, a single-degree of freedom oscillator with discontinuous support is analyzed. An experimental apparatus is developed in order to verify the capability of the mathematical formulation and the numerical procedure used to describe the system general behavior. This apparatus is instrumented to obtain all system state variables, making it possible to compare experimental results with those obtained through numerical simulations. The system's dynamical behavior shows a rich response that includes dynamical jumps, bifurcations and chaos. Different aspects related to nonlinear dynamics are carried out showing that numerical simulations are in close agreement with experimental data.

1. Introduction

Non-smooth nonlinearity is abundant in nature and is usually related to either friction phenomena or the discontinuous characteristics of intermittent contacts between some system components. Non-smooth systems appear in many kinds of engineering systems and also in everyday life. Examples include the stick-slip oscillations of a violin string or grating brakes [1]. Some related phenomena such as chatter and squeal cause serious problems in many industrial applications and, in general, these forms of vibrations are undesirable because of their detrimental effects on the operation and performance of mechanical systems [2].

*Corresponding author. Tel.: +55 21 2562 8372; fax: +55 21 2562 8383.
E-mail addresses: savi@mecanica.ufrj.br (M.A. Savi), Luiz.Franca@csiro.au (L.F.P. Franca), hans@mec.puc-rio.br (H.I. Weber).

0022-460X/$ - see front matter © 2006 Elsevier Ltd. All rights reserved.
doi:10.1016/j.jsv.2006.09.014

The mathematical modeling and numerical simulations of non-smooth systems present many difficulties, which makes their description unusually complex. Moreover, the dynamical behavior of these systems is complex resulting in a rich set of responses. In the literature there are many reports dealing with non-smooth systems. In general, they are focused on the mathematical modeling, proper numerical algorithms to treat these systems, and also experimental approaches employed in order to verify the obtained results. In all of these works, it should be pointed out that highly complex dynamical responses result from these non-smooth system characteristics.

Andreaus and Casini [2] analyze the response of a single-degree of freedom (dof) system with dry friction under a constant velocity of the base and/or the harmonic driving force. In this article different friction models using standard numerical procedures are considered. Hinrichs et al. [1,3] analyze a system with dry friction both by numerical and by experimental approaches. The authors suggest that an extension of the friction model is necessary in order to fully understand the non-smooth transition points of the trajectories. Peterka [4] studied a double impact oscillator represented by two symmetrically arranged single impact oscillators. The anti-phase impact motion of this system has dynamics identical to those of the single system. The in-phase motion and the influence of asymmetries of the system parameters are studied through numerical simulations. An experimental apparatus was used to verify the obtained results.

The importance of grazing effects in non-smooth systems related to contact interactions, in particular those of frictional origin, is the objective of many research efforts. Nordmark's [5] was probably the first important work in this area. Pavlovskaia et al. [6] and Dankowicz and Nordmark [7] analyzed discontinuous oscillators that they proposed to examine impact phenomenon. Virgin and Begley [8] showed that grazing bifurcations are intimately associated with the evolution of basins of attraction when a system parameter changes.

The idea that non-smooth systems can be considered as continuous in a finite number of continuous subspaces and also that the system parameters do not change in an abrupt manner, inspires some authors to try to describe non-smooth systems by a smoothed form. Refs. [9–14] are some articles where interesting approaches are proposed in order to deal with mathematical discontinuity.

Since non-smooth systems present an unusually complex behavior and their description involves many mathematical and numerical difficulties, experimental studies are of great importance. Some of the authors of the cited references used experimental approaches to verify the proposed numerical methods. Others just discuss experimental results. Wiercigroch and co-workers [15,16] present an experimental analysis of a base excited symmetrically bilinear oscillator. Virgin and co-workers also performed interesting analyses related to non-smooth systems [17–21].

The objective of this research effort is the nonlinear dynamics analysis of a single-dof system with discontinuous support. Despite the deceiving simplicity of this problem, its nonlinear dynamics is very rich. Numerical and experimental approaches are employed. The mathematical model uses a smoothened switch model [9,10], which treats non-smooth systems by defining different sets of ordinary differential equations. The smoothed system is built defining transition equations of motions that govern the dynamical response during the transition from one set to another. Therefore, the state space is split into subspaces each governed by their own smooth ordinary differential equation. The use of this approach smoothes discontinuities and allow one to employ classical numerical procedures within each subspace. By using this approach, numerical investigations of the behavior of a single-dof system with a discontinuous support are efficient, and thus many different aspects of the non-smooth system dynamics can be examined [22].

In order to verify numerical results, an experimental apparatus was constructed. Basically, the apparatus is composed of an oscillator which is a car, free to move over a rail, connected to an excitation system. The discontinuous support construction involves a spring whose position can be changed relative to the car position so that the effect of different gap sizes can be examined. This apparatus is instrumented to obtain all system state variables, making it possible to compare experimental results with those obtained in numerical simulations. In general, numerical and experimental results are in close agreement.

2. Discontinuous support model

The dynamical response of a single-dof system with discontinuous support, shown in Fig. 1, is analyzed. The oscillator is composed by a mass m and two linear springs with stiffness k. The dissipation process may be

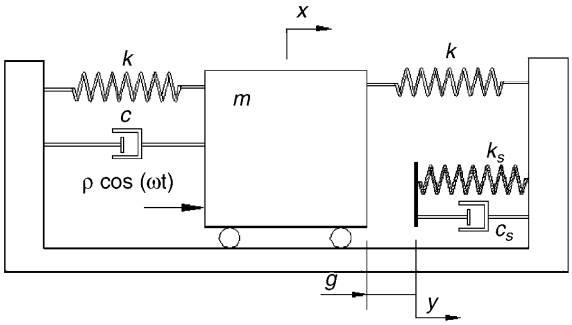

Fig. 1. Non-smooth system with discontinuous support.

modeled by a linear velocity dependent damping element with coefficient c. Moreover, the support is massless, having a linear spring with stiffness k_s and, again, the dissipation process is represented by a linear damping element with coefficient c_s. The mass displacement is denoted by x, relative to the equilibrium position, while the support displacement is denoted by y. The distance between the mass and the support is defined by a gap g. Therefore, the system has two possible modes of operation: either the mass is in contact with the support or there is no contact. Denoting the contact force between the mass and the support by f_s, these two situations may be represented as follows:

$$\begin{cases} x < g \ \text{ and } \ f_s = 0 \quad \text{(without contact)}, \\ x \geqslant g \ \text{ and } \ f_s = -(k_s y + c_s \dot{y}) < 0 \quad \text{(with contact)}. \end{cases} \tag{1}$$

The support relaxes to the equilibrium state when there is no contact between the mass and the support. By assuming that the support relaxation time is much smaller than the time between two contact events, the support dynamics can be neglected. This assumption reduces the system dynamics to a second-order differential equation associated with the dynamics of the mass-spring-dashpot. Therefore, the governing equations may be defined by two different equations, representing situations with and without contact. Under these assumptions, and assuming that this system is subjected to a harmonic excitation, $\rho \cos(\omega t)$, the equations of motions are given by

$$\begin{cases} m\ddot{x} + 2kx + c\dot{x} = \rho \cos(\omega t) \quad \text{(without contact)}, \\ m\ddot{x} + 2kx + k_s(x - g) + (c + c_s)\dot{x} = \rho \cos(\omega t) \quad \text{(with contact)}. \end{cases} \tag{2}$$

According to the Filippov theory [9,10,22,23], the phase space of this type of system $\dot{u} = \tilde{f}(u)$, $u = (x, \dot{x})$ may be split into two subspaces $\tilde{\Gamma}_-$ and $\tilde{\Gamma}_+$, separated by a hyper-surface $\tilde{\Sigma}$, which is defined by a scalar indicator function $h(u)$. In order to use Filippov's approach to the modeling of the oscillator shown in Fig. 1, it is necessary to develop a proper description of the transitions. The contact between the mass and the support occurs if the displacement becomes equal to the gap g. On the other hand, the mass loses contact with the support when the contact force vanishes, i.e., if $f_s = -[k_s(x - g) + c_s\dot{x}] = 0$. Therefore, there are two subspaces with two different transition situations. The subspaces are defined by two indicator functions:

$$\begin{aligned} h_\alpha(x, \dot{x}) &= x - g, \\ h_\beta(x, \dot{x}) &= -(x - g) - \frac{c_s}{k_s}\dot{x}. \end{aligned} \tag{3}$$

Now, it is possible to describe the mass motion, considering that there is no contact with the support if the state vector $u = (x, \dot{x}) \in \tilde{\Gamma}_-$. On the other hand, there is contact between the mass and the support if $u = (x, \dot{x}) \in \tilde{\Gamma}_+$. These situations are represented by the following sets:

$$\tilde{\Gamma}_- = \left\{ u \in R^2 / h_\alpha(u) < 0 \ \text{ or } \ h_\beta(u) > 0 \right\}, \tag{4a}$$

$$\tilde{\Gamma}_+ = \left\{ u \in R^2 / h_\alpha(u) > 0 \ \text{ and } \ h_\beta(u) < 0 \right\}. \tag{4b}$$

The transitions are related to a hyper-surface $\tilde{\Sigma}$, which consists of the conjunction of two surfaces $\tilde{\Sigma}_\alpha$ and $\tilde{\Sigma}_\beta$. The hyper-surface $\tilde{\Sigma}_\alpha$ defines the transition from $\tilde{\Gamma}_-$ to $\tilde{\Gamma}_+$, representing situations where the contact is caused when x becomes greater than g. On the other hand, the hyper-surface $\tilde{\Sigma}_\beta$ defines the transition from $\tilde{\Gamma}_+$ to $\tilde{\Gamma}_-$ as the contact is lost when the force of the support vanishes. Therefore,

$$\tilde{\Sigma}_\alpha = \left\{u \in R^2 / h_\alpha(u) = 0 \text{ and } h_\beta(u) \leqslant 0\right\}, \tag{5a}$$

$$\tilde{\Sigma}_\beta = \left\{u \in R^2 / h_\alpha(u) > 0 \text{ and } h_\beta(u) = 0\right\}. \tag{5b}$$

This non-smooth system may be smoothed by redefining the subspaces and the transition hyper-surfaces. Therefore, it is assumed that the transition has a linear variation within Σ_α (from $\tilde{f}_-$ to $\tilde{f}_+$), and also within Σ_β (from $\tilde{f}_+$ to $\tilde{f}_-$), which is related to a thin space defined by a narrow band η around the hyper-surface of discontinuity. The subspaces and the hyper-surfaces related to the single-dof dynamics, for both the non-smooth and smoothed systems, are shown in Fig. 2.

The definition of the transitions is made assuming that the dynamics through a η narrow band is governed by $f_\alpha = (1-q)f_- + qf_+$ with $q = (x-g+\eta)/2\eta$ within the subspace Σ_α and by $f_\beta = (1-q)f_+ + qf_-$ with $q = [-x+g+\eta-(c_s/k_s)\dot{x}]/2\eta$ within Σ_β (note that $0 \leqslant q \leqslant 1$ in both cases). In order to define these transitions it is assumed that there is a time instant t_a where $q = 0$, the input limit of region Σ_α, and also a time instant t_b where $q = 1$, the output limit of region Σ_α. In an analogous form, there is a time instant t_c where $q = 0$, the input limit of region Σ_β, and also a time instant t_d where $q = 1$, the output limit of region Σ_β. Therefore, the system dynamics can be written as follows [10,22]:

$$\dot{u} = f(u,t) = \begin{cases} f_-, & u \in \Gamma_-, \\ f_\alpha, & u \in \Sigma_\alpha, \\ f_\beta, & u \in \Sigma_\beta, \\ f_+, & u \in \Gamma_+, \end{cases} \tag{6}$$

where

$$f_-(u,t) = \left\{ \begin{array}{c} \dot{x} \\ -\dfrac{2k}{m}x - \dfrac{c}{m}\dot{x} + \dfrac{\rho}{m}\cos(\omega t) \end{array} \right\}, \tag{7a}$$

$$f_+(u,t) = \left\{ \begin{array}{c} \dot{x} \\ -\dfrac{2k}{m}x - \dfrac{k_s}{m}(x-g) - \dfrac{c+c_s}{m}\dot{x} + \dfrac{\rho}{m}\cos(\omega t) \end{array} \right\}, \tag{7b}$$

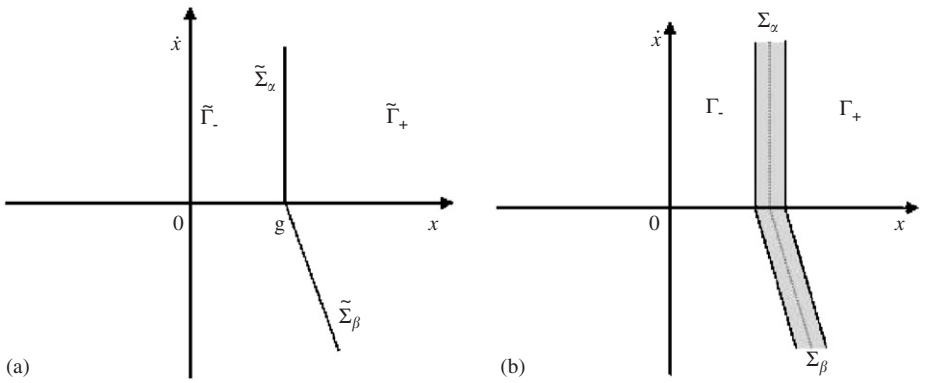

Fig. 2. Subspaces related to the system dynamics: (a) non-smooth system and (b) smoothed system.

and the transitions associated with hyper-surfaces Σ_α and Σ_β are given by

$$f_\alpha = \left\{ \begin{array}{c} \dot{x} \\ -\dfrac{2k}{m}x - \dfrac{c+c_s}{m}\dot{x} + \dfrac{\rho}{m}\cos(\omega t) - \dfrac{k_s}{2m}(x-g+\eta) + \dfrac{c_s}{m}\dot{x}_a\left(1 - \dfrac{x-g+\eta}{2\eta}\right) \end{array} \right\}, \tag{8a}$$

$$f_\beta = \left\{ \begin{array}{c} \dot{x} \\ -\dfrac{2k}{m}x - \dfrac{c}{m}\dot{x} + \dfrac{\rho}{m}\cos(\omega t) - \dfrac{k_s}{2m}(x-g+\eta) - \dfrac{c_s}{2m}\dot{x} \end{array} \right\}. \tag{8b}$$

Note that $\dot{x}_a$, the velocity in time instant t_a, is used in these equations. The subspaces and transition hyper-surfaces are now represented by the following sets:

$$\Gamma_- = \left\{u \in R^2 / h_\alpha(u) \leqslant -\eta \ \text{ or } \ h_\beta(u) \geqslant \eta\right\}, \tag{9a}$$

$$\Gamma_+ = \left\{u \in R^2 / h_\alpha(u) \geqslant \eta \ \text{ and } \ h_\beta(u) \leqslant -\eta\right\}, \tag{9b}$$

$$\Sigma_\alpha = \left\{u \in R^2 / -\eta < h_\alpha(u) < +\eta \ \text{ and } \ h_\beta(u) \leqslant -h_\alpha(u)\right\}, \tag{10a}$$

$$\Sigma_\beta = \left\{u \in R^2 / h_\alpha(u) > -h_\beta(u) \ \text{ and } \ -\eta < h_\beta(u) < +\eta\right\}. \tag{10b}$$

This approach allows one to deal with non-smooth systems by employing a smoothened system. The thickness parameter of the narrow band η need to be appropriately chosen for each physical problem [10,22]. This switch model is introduced as an appropriate procedure to perform numerically efficient mathematical modeling of non-smooth system behavior [22].

3. Experimental apparatus

In order to perform an experimental analysis of a non-smooth system, an experimental apparatus of the single-dof oscillator discussed in the previous section was constructed. With reference to Fig. 3, the apparatus is composed of a car (4), free to move over a rail (2), connected to an excitation system composed of springs (3), strings and a DC motor (1) (PASCO ME-8750 with 0–12 V e 0–0.3 A). Moreover, the apparatus has an adjustable magnetic damping device (5). The discontinuous support (6) is constructed using a spring whose

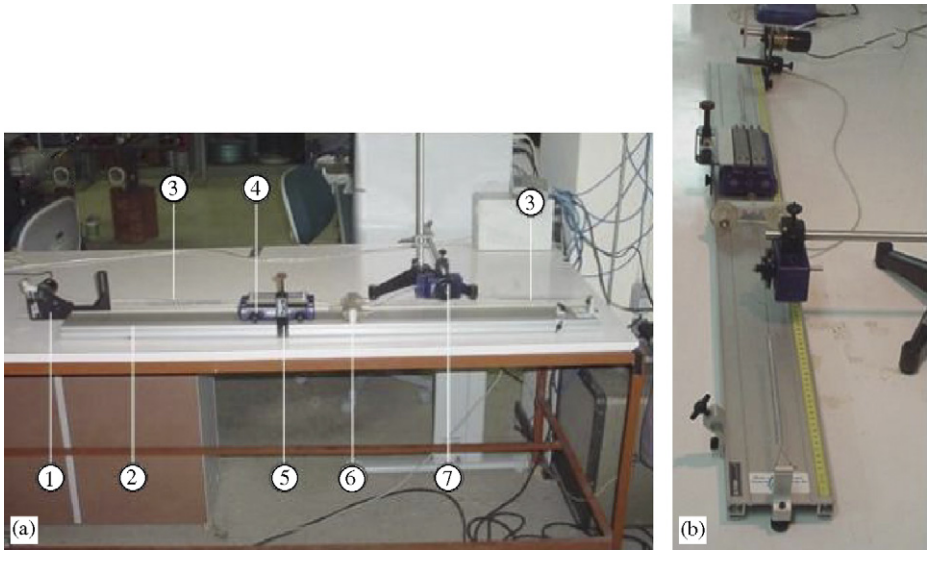

Fig. 3. Experimental apparatus: (a) side view and (b) end view. (1) DC motor, (2) rail, (3) spring, (4) car, (5) damping device, (6) support and (7) rotary sensor.

position can be adjusted to change the gap between the support and the car position. The movement is measured with the aid of a rotary sensor (7), PASCO CI-6538, which has a precision of ± 0.25 degrees, a maximum velocity of 30 rev/s and a maximum sampling frequency of 1000 Hz.

The behavior of this device is controlled by parameters related to the oscillator and also to the support, as shown in the modeling presented in the previous section. Besides the mass, m, there are the stiffnesses of the main springs, k, and of the support, k_s. Moreover, there are the parameters related to the dissipation of the oscillator, c, and of the support, c_s. The other important characteristics of the system are the gap, g, the excitation frequency, ω, and the amplitude of the excitation, ρ. The estimation of these parameters is discussed in the following section.

In addition to the transducers employed to measure the state variables, a force transducer (PS-2104), which has a range of ± 50 N with 1% of accuracy and resolution of 0.03 N, is used in the estimation of the spring stiffness which is performed by calculating the slope of a force-displacement curve. All measurements are made at a sample rate of 100 Hz.

3.1. Parameter estimation

The system mass was measured with a weight scale, and found to be $m = 0.838$ kg. The stiffness values were estimated by using different procedures. First, the stiffness was estimated by determining the slope of a force–displacement curve, generated with the aid of two sensors: the rotary sensor shown in Fig. 3 and a force transducer. These results are shown in Fig. 4. The oscillator was found to have a stiffness (k) of 8.47 N/m, while the support (k_s) stiffness was calculated to be 1210 N/m.

Just as a verification of these measurements, the system natural frequency was also estimated. Since $\omega_0 = \sqrt{k/m}$, it is possible to confirm the oscillator stiffness. By using the measures of the mass and the stiffness one has, $\omega_0 = 4.50$ rad/s. This value may also be obtained from the examination of the magnitude of the Discrete Fourier Transform (DFT) of the sampled impulsive response. The response time history and the magnitude of the DFT are shown in Fig. 5. The undamped natural frequency (ω_0) was estimated to be 4.60 rad/s, which is near to the previous result.

The magnetic device responsible for the system dissipation may be modeled by a combination of linear viscous damping and dry friction. In the considered range, the dry friction may be neglected and, therefore, the estimation of the oscillator dissipation parameter, c or $\xi = c/2m\omega_0$, may be done by analyzing the system frequency response. The idea is to fit the maximum amplitude obtained by numerical simulations with those obtained in the experiments by adjusting the dissipation parameter. The prediction of the response from the estimated model ($\xi = 0.115$ or $c = 2\xi m\omega_0 = 0.87$ Ns/m) is shown in Fig. 6 along with experimental results.

The support dissipation parameter is identified connecting the support to a mass and analyzing its free response. By using a logarithmic decrement procedure, the damping coefficient was estimated. This technique is based on the relationship between ξ and the ratio between any two consecutive displacement amplitudes. Therefore, by analyzing the impulsive response of the system shown in Fig. 7, it is possible to employ classical expressions in order to estimate c_s as 0.60 Ns/m i.e., $\xi_s = 0.0075$.

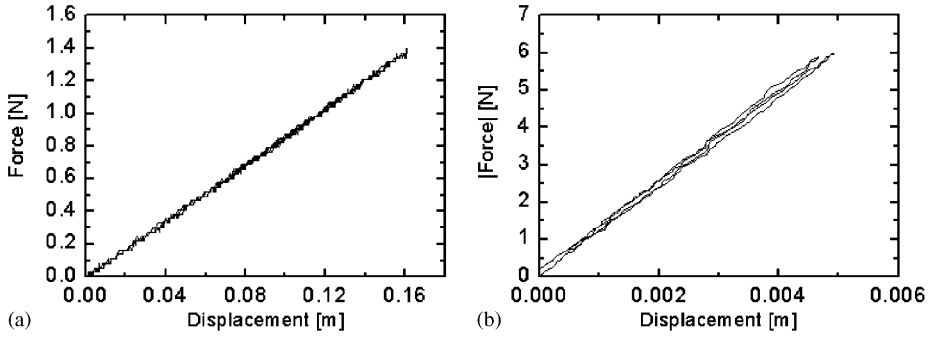

Fig. 4. Spring stiffness: (a) oscillator ($k = 8.47$ N/m) and (b) support ($k_s = 1210$ N/m).

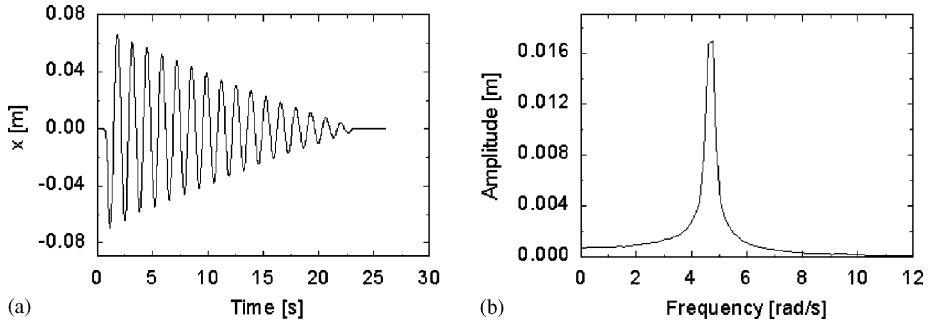

Fig. 5. Evaluation of the natural frequency: (a) displacement time history and (b) magnitude of discrete Fourier transform (peak at 0.732 Hz or 4.60 rad/s).

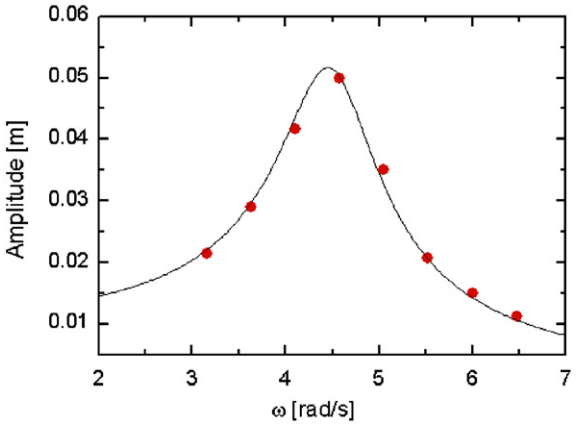

Fig. 6. Determination of dissipation parameter by considering the maximum displacement for different frequencies ($\xi = 0.115$). ● Experimental and — Numerical.

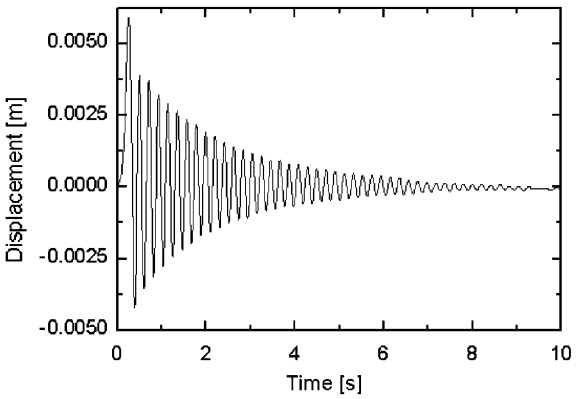

Fig. 7. Impulsive response of the support connected to a mass: $m = 1.33$ kg, $\xi_s = 0.0075$ and $c_s = 0.60$ Ns/m.

Now, the excitation characteristic is focused on. Initially, the frequency excitation is analyzed, establishing a relation between this frequency and the DC motor voltage. Moreover, the forcing amplitude is evaluated by defining a relation between this force and the motor position, which is related to the length of rotating crank, a. The voltage–frequency curve and also the forcing amplitude–motor position curve are shown in Fig. 8. The

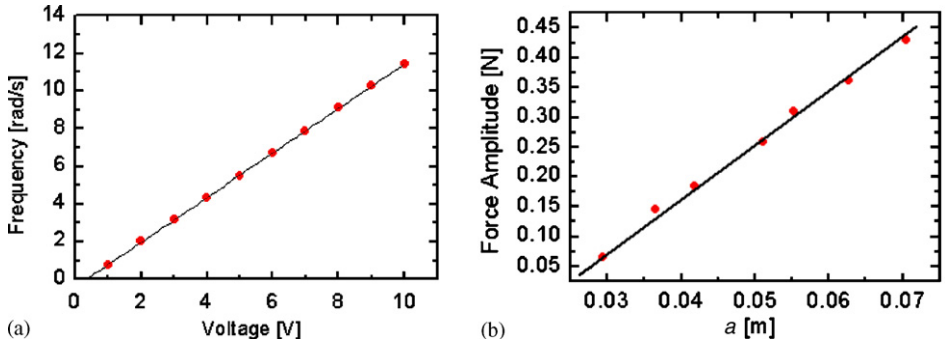

Fig. 8. (a) Voltage–frequency curve and (b) length of rotating crank-forcing amplitude. ● Experimental and — fitted curve.

Table 1
System parameters experimentally identified

k (N/m)	k_s (N/m)	c (Ns/m)	c_s (Ns/m)	m (kg)	ω_0 (rad/s)
8.47	1210	0.87	0.60	0.838	4.60

relationship between the force and the motor position is examined with the aid of a force transducer (PS-2104).

The parameter estimates derived from fitting the model to the experimental data are shown in Table 1.

4. Numerical and experimental results

Numerical and experimental investigations of the system that includes discontinuous support are described in this section. Parameters experimentally identified, as described in the previous section, are used in all simulations. The proposed mathematical formulation is integrated with the aid of the Runge–Kutta–Fehlberg method, and for this numerical parameters need to be chosen properly. Divenyi et al. [23] show the importance of the choice of the narrow band thickness η, which is related to the proper transition of the system response in subspaces Γ_- and Γ_+, and also the hyper-surfaces Σ_α and Σ_β. On this basis, it is assumed that $\eta = 10^{-5}$ for all simulations.

A comparison between numerical and experimental results is now of concern. At first, frequency domain analysis is focused on considering the resonance curve of the system with discontinuous support assuming $\rho = 0.14\,\mathrm{N}$ and $g = 0.02\,\mathrm{m}$ (Fig. 9). The resonance curve has a typical characteristic of nonlinear systems: dynamical jumps that occur at different locations when increasing and decreasing the frequency of excitation. Therefore, in order to analyze these jumps, two situations are considered: in the first one the excitation frequency is increasing while in the second situation the frequency is decreasing. First of all, it should be pointed out that the numerical and experimental results are in close agreement. Besides, by observing the frequency increase, notice that there is a small period-2 region near $\omega = 3.63\,\mathrm{rad/s}$, and after that, a dynamical jump occurs near $\omega = 5.88\,\mathrm{rad/s}$. In contrast, when decreasing the excitation frequency, the dynamical jump occurs in a different position, at $\omega = 5.29\,\mathrm{rad/s}$, and after that, the period-2 response appears again. Note that there is also an unstable region between the frequencies where the jumps associated with frequency increases and decreases occur.

The frequency response for a different set of forcing parameters, $\rho = 0.16\,\mathrm{N}$ and $g = 0.0145\,\mathrm{m}$, are presented in Fig. 10. These results have the similar behavior to that seen in the previous case. Nevertheless, notice that, for this set of parameters, the period-2 response does not exist anymore and, instead of that, there is a small jump. Both behaviors are probably related to the grazing phenomenon, discussed later.

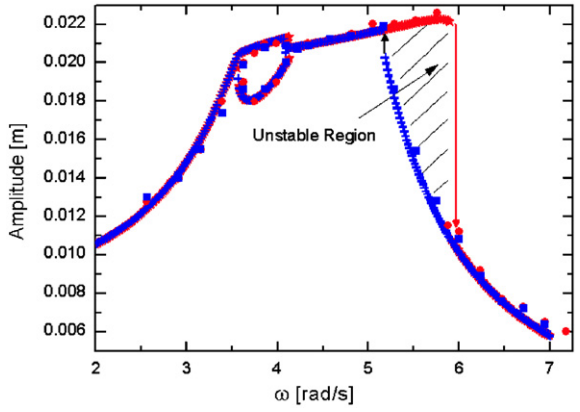

Fig. 9. Frequency response for $\rho = 0.14\,\mathrm{N}$ and $g = 0.02\,\mathrm{m}$. ✻ Numerical increasing, + numerical decreasing, ● experimental increasing and ■ experimental decreasing.

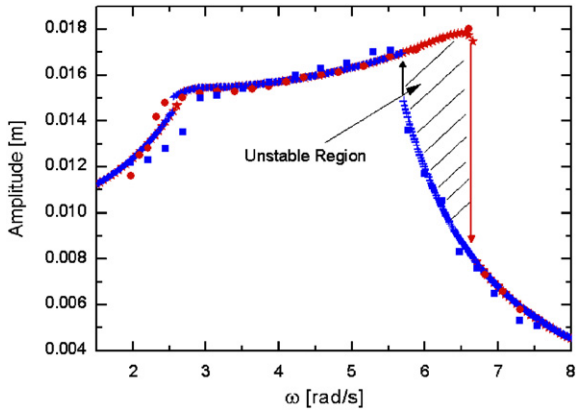

Fig. 10. Frequency response for $\rho = 0.16\,\mathrm{N}$ and $g = 0.0145\,\mathrm{m}$. ✻ Numerical increasing, + numerical decreasing, ● experimental increasing and ■ experimental decreasing.

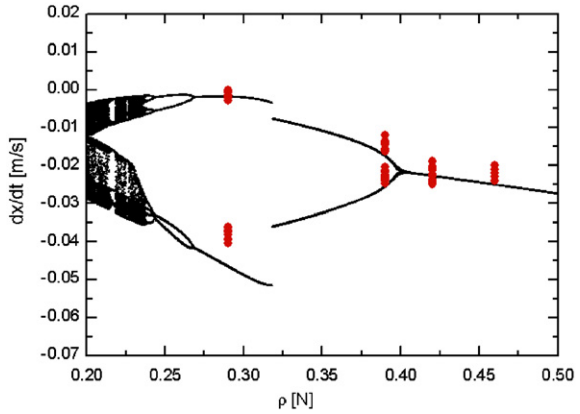

Fig. 11. Bifurcation diagram for $\omega = 3.69\,\mathrm{rad/s}$ and $g = -0.0045\,\mathrm{m}$, varying the forcing amplitude. ● Experimental and • numerical.

At this point, the influence of the forcing amplitude in the system dynamics is considered. A bifurcation diagram representing the stroboscopically sampled velocity values under the slow quasi-static increase of the driving force amplitude is used with $\omega = 3.69\,\mathrm{rad/s}$, $g = -0.0045$, and $0.2 \leqslant \rho \leqslant 0.5\,\mathrm{N}$ (Fig. 11). Again,

numerical and experimental results are in close agreement, showing period-1 responses ($\rho \geqslant 0.406$), period-2 responses ($0.28 \leqslant \rho \leqslant 0.406$), period-4 responses ($0.26 \leqslant \rho \leqslant 0.28$) and also chaotic responses ($\rho \leqslant 0.26$ N). The small discrepancies between the numerical and experimental results are probably due to differences in the Poincaré section position. Phase space plots and the associated Poincaré maps, for different values of forcing amplitude parameters, $\rho = 0.29$, 0.39, 0.42 and 0.46, are presented in Fig. 12.

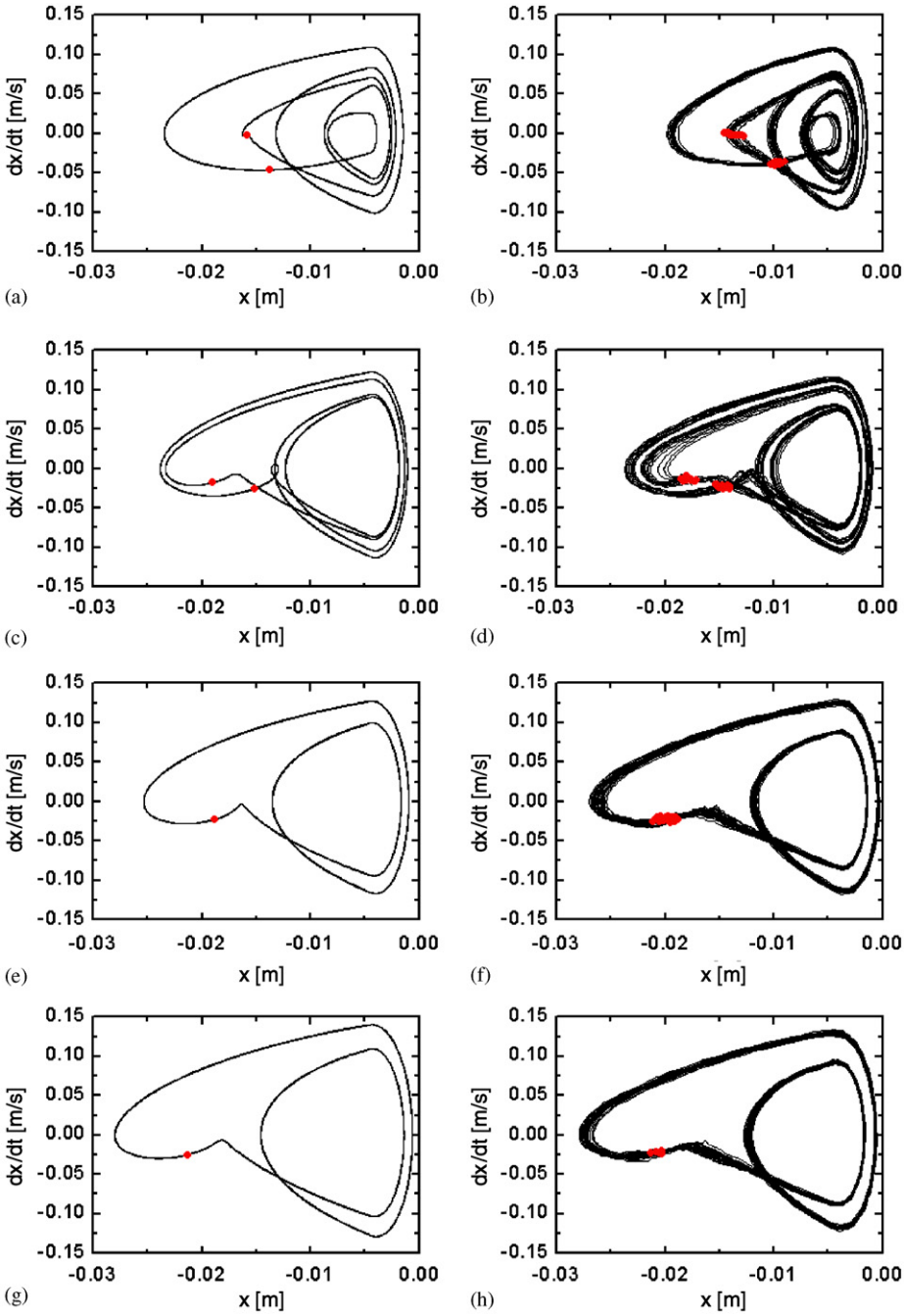

Fig. 12. State space and Poincaré section comparing numerical and experimental results. Numerical—$\rho = 0.29$ N, (b) experimental—$\rho = 0.29$ N, (c) numerical—$\rho = 0.39$ N, (d) experimental—$\rho = 0.39$ N, (e) numerical—$\rho = 0.42$ N, (f) experimental—$\rho = 0.42$ N, (g) numerical—$\rho = 0.46$ N and (h) experimental—$\rho = 0.46$ N. — Phase space and ● Poincaré sections.

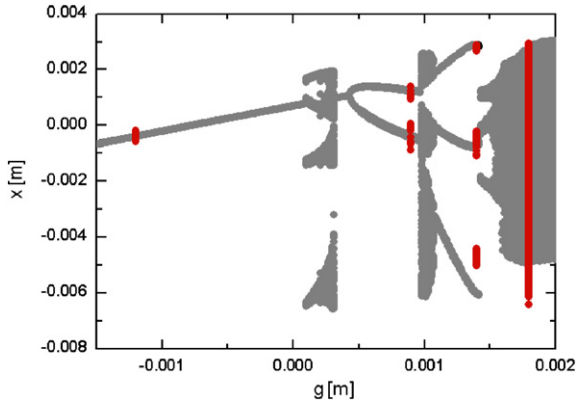

Fig. 13. Bifurcation diagram for $\omega = 11.15$ rad/s and $\rho = 0.33$ N, varying gap. ● Numerical and ● experimental sections ($g = -0.0012$, 0.0009, 0.0014 and 0.0018 m).

Now, the gap influence is focused on. In this analysis, it is assumed that $\omega = 11.15$ rad/s and $\rho = 0.33$. The gap varies in the range $-0.0015 \leqslant g \leqslant 0.002$ m, and the corresponding bifurcation diagram is shown in Fig. 13. Again, it should be pointed out that there is good agreement between numerical and experimental results, both show periodic and chaotic responses. The phase space for different values of the gap, $g = -0.0012$, 0.005, 0.0012 and 0.0014 m, showing, respectively, period-1, period-2, period-3 and chaotic responses, are presented in Fig. 14.

Strange attractors related to the chaotic response in the previous simulations ($g = 0.0018$ m) are presented in Figs. 15 and 16, different Poincaré section positions are shown in plots (a)–(d). Numerical simulation results are presented in Fig. 15 while results obtained from the experimental apparatus are presented in Fig. 16. Once again, note the agreement between them.

The importance of grazing effects in non-smooth systems related to contact interactions, in particular those of frictional origin, is the objective of many research efforts. Grazing orbits occur when the phase space orbit touches lightly the boundary. Under this condition, a further incremental change to the excitation characteristics produces contact behavior that is not easily predicted. For some combination of system parameters, the response may proceed abruptly into or out the chaos. This unpredictability related to grazing bifurcations constitutes a typical behavior of non-smooth systems that does not appear in smooth systems [5–8,22,24,25].

A brief examination of the grazing phenomenon and the different kinds of motion associated with it is given below. On this basis, bifurcation diagrams associated with the position and displacement, with $\rho = 0.23$ N and $g = 0.0036$, are generated by varying the frequency parameter ω (Fig. 17). From these diagrams, it can be seen that there is a periodic response when there is no contact when $\omega = 8.64$ rad/s, a chaotic response when $\omega = 9.55$ rad/s, and another periodic response when there is contact for $\omega = 9.88$ rad/s. It should also be pointed out that there is an abrupt transition from the periodic to chaotic response and, afterwards, from the chaotic to the periodic response. The phase spaces related to these frequencies are shown in Fig. 18, together with the experimental results.

5. Conclusions

The analysis of a non-smooth system with discontinuous support, considering both numerical and experimental approaches, is presented in this contribution. A single-dof oscillator with discontinuous support is analyzed as an application of this kind of system. In the mathematical modeling of this system a smoothed switch model is assumed that splits the phase space into subspaces, defining finite regions to describe transitions between them. This procedure is useful for numerical simulations and is an effective form for integration of the non-smooth equations. Moreover, an experimental apparatus was constructed in order to

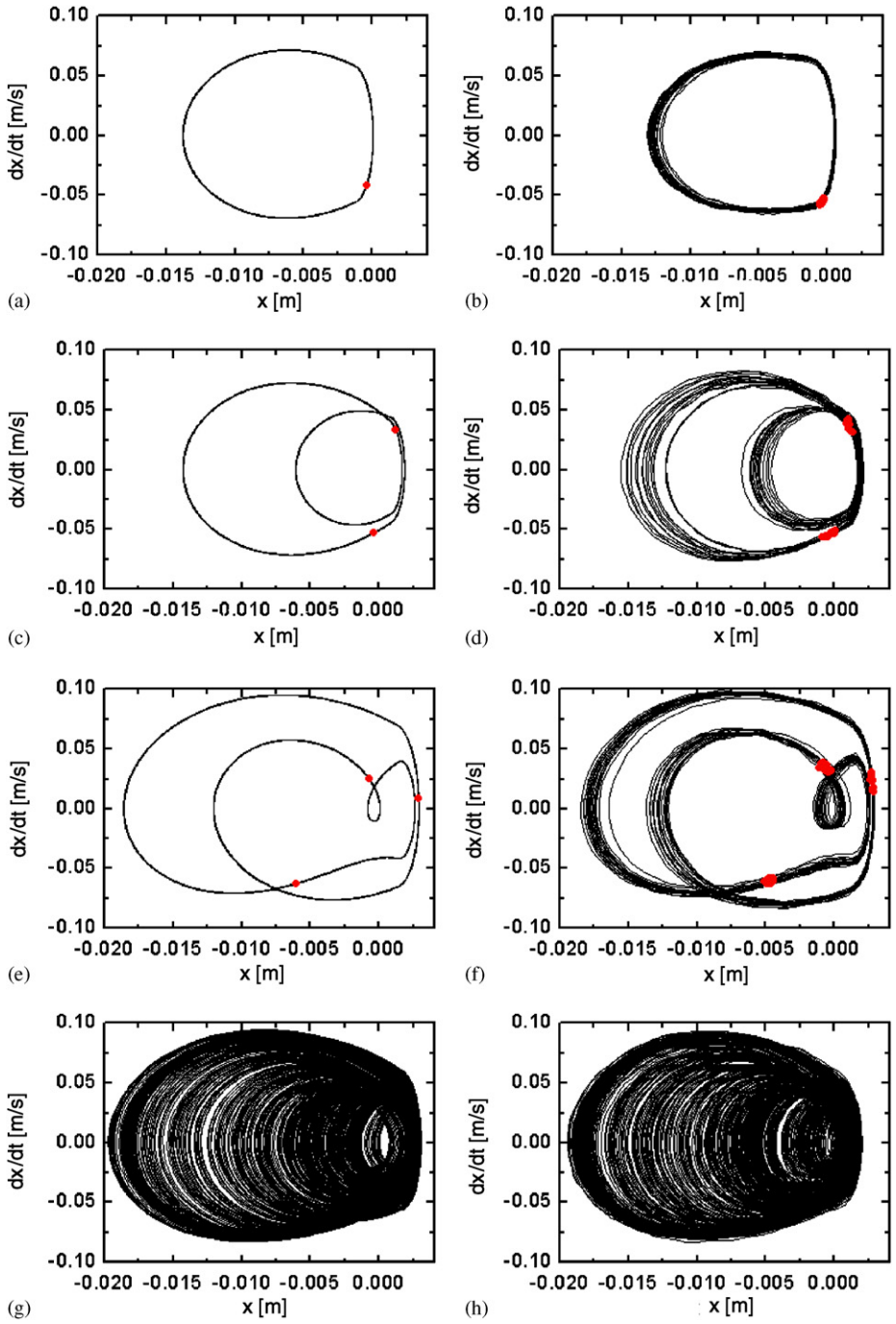

Fig. 14. State space comparing numerical and experimental results. (a) Numerical—$g = -0.0012$ m, (b) experimental—$g = -0.0012$ m, (c) numerical—$g = 0.0009$ m, (d) experimental—$g = 0.0009$ m, (e) numerical—$g = 0.0014$ m, (f) experimental—$g = 0.0014$ m, (g) numerical—$g = 0.0018$ m and (h) experimental—$g = 0.0018$ m. — Phase space; ● Poincaré sections (not present in (g) and (h)).

verify the numerical results. Basically, the apparatus is composed of a car, free to move over a rail, connected to an excitation system through a spring. The discontinuous support is a spring whose end point can be positioned to vary the gap between it and the car position. This apparatus was instrumented to obtain all the

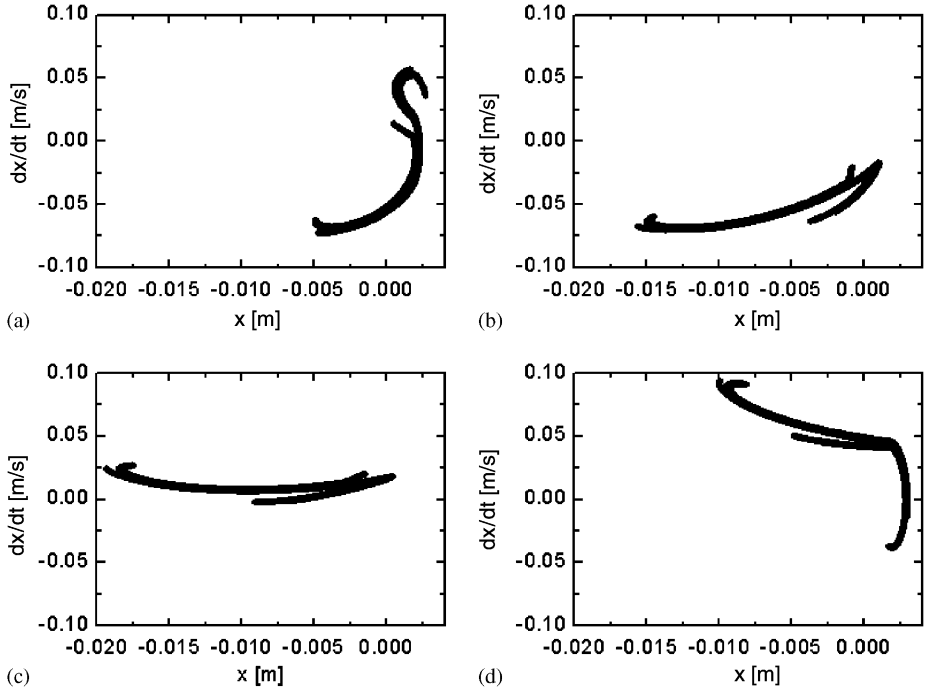

Fig. 15. Chaotic attractors related to numerical simulations and different Poincaré section positions, $\rho = 0.33\,\mathrm{N}$, $\omega = 11.15\,\mathrm{rad/s}$ and $g = 0.0018\,\mathrm{m}$. (a) 0, (b) $\pi/2$, (c) π and (d) $3\pi/2$.

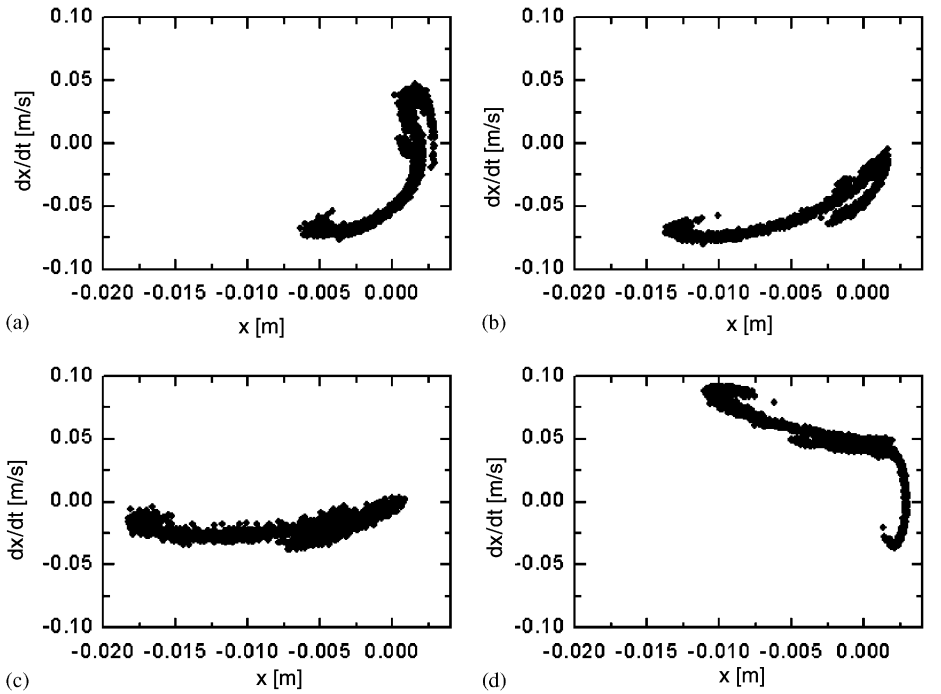

Fig. 16. Chaotic attractors related to experimental setup and different Poincaré section positions, $\rho = 0.33\,\mathrm{N}$, $\omega = 11.15\,\mathrm{rad/s}$ and $g = 0.0018\,\mathrm{m}$. (a) 0, (b) $\pi/2$, (c) π and (d) $3\pi/2$.

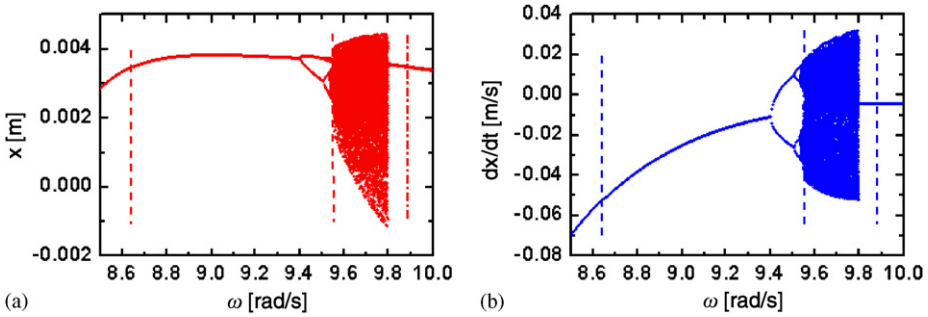

Fig. 17. Bifurcation diagram $\rho = 0.23\,\mathrm{N}$ and $g = 0.0036\,\mathrm{m}$, varying frequency parameter: (a) displacement and (b) velocity. Highlighted sections: $\omega = 8.64$, 9.55 and 9.88 rad/s.

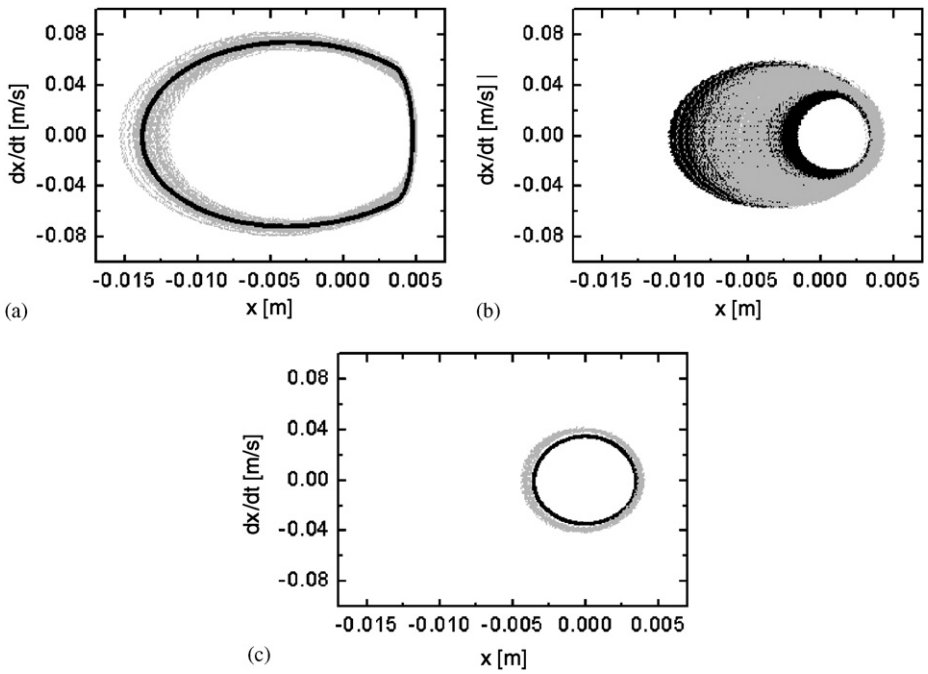

Fig. 18. Phase spaces for $\rho = 0.23\,\mathrm{N}$ and $g = 0.0036\,\mathrm{m}$. (a) Periodic response ($\omega = 8.64$ rad/s), (b) chaotic response ($\omega = 9.55$ rad/s) and (c) periodic response ($\omega = 9.88$ rad/s). ▲ Numerical and ● experimental.

system state variables, making it possible to compare the experimental results with those obtained in numerical simulations. After estimation of the system parameters, numerical and experimental investigations were carried out allowing examination of different characteristics of the system dynamics. In general, numerical and experimental results are in close agreement. Very rich dynamics are observed in both approaches, including dynamical jumps, bifurcations and chaos. The grazing bifurcation that causes abrupt changes in the system response is revealed to be an important characteristic of this kind of system. Finally, the authors believe that the proposed procedure may be useful for the analysis of other non-smooth systems.

Acknowledgements

The authors would like to acknowledge the support of the Brazilian Research Council (CNPq).

References

[1] N. Hinrichs, M. Oestreich, K. Popp, On the modelling of friction oscillators, *Journal of Sound and Vibration* 216 (3) (1998) 435–459.
[2] U. Andreaus, P. Casini, Dynamics of friction oscillators excited by a moving base and/or driving force, *Journal of Sound and Vibration* 245 (4) (2001) 685–699.
[3] N. Hinrichs, M. Oestreich, K. Popp, Dynamics of oscillators with impact and friction, *Chaos, Solitons & Fractals* 8 (4) (1997) 535–558.
[4] F. Peterka, Dynamics of double impact oscillators, *FACTA Univresitatis—Mechanics, Automatic Control and Robotics* 2 (10) (2000) 1177–1190.
[5] A.B. Nordmark, Non-periodic motion caused by grazing incidence in an impact oscillator, *Journal of Sound and Vibration* 145 (1991) 279–297.
[6] E. Pavlovskaia, M. Wiercigroch, C. Grebogi, Modeling of an impact system with a drift, *Physical Review E* 64 (2001) 056–224.
[7] H. Dankowicz, A.B. Nordmark, On the origin and bifurcations of stick-slip oscillations, *Physica D* 136 (2000) 280–302.
[8] L.N. Virgin, C.J. Begley, Grazing bifurcations and basins of attraction in an impact-friction oscillator, *Physica D* 130 (1999) 43–57.
[9] M. Wiercigroch, Modelling of dynamical systems with motion dependent discontinuities, *Chaos, Solitons & Fractals* 11 (2000) 2429–2442.
[10] R.I. Leine, Bifurcations in discontinuous mechanical systems of Filippov-type, Ph.D. Thesis, Technische Universiteit Eindhoven, 2000.
[11] R.I. Leine, D.H. van Campen, B.L. van de Vrande, Bifurcations in nonlinear discontinuous systems, *Nonlinear Dynamics* 23 (2000) 105–164.
[12] R.I. Leine, D.H. van Campen, B.L. van de Vrande, Bifurcations in nonlinear discontinuous systems, *Nonlinear Dynamics* 23 (2000) 105–164.
[13] R.I. Leine, D.H. van Campen, Discontinuous bifurcations of periodic solutions, *Mathematical and Computer Modelling* 36 (2002) 259–273.
[14] R.I. Leine, D.H. van Campen, Discontinuous fold bifurcation in mechanical systems, *Archive of Applied Mechanics* 72 (2002) 138–146.
[15] M. Wiercigroch, V.W.T. Sin, K. Li, Measurement of chaotic vibration in a symmetrically piecewise linear oscillator, *Chaos, Solitons & Fractals* 9 (1/2) (1998) 209–220.
[16] M. Miercigroch, V.W.T. Sin, Experimental study of a symmetrical piecewise base-excited oscillator, *Journal of Applied Mechanics—ASME* 65 (1998) 657–663.
[17] M.D. Todd, L.N. Virgin, Natural frequencies considerations of an impact oscillator, *Journal of Sound and Vibration* 194 (3) (1996) 452–460.
[18] M.D. Todd, L.N. Virgin, An experimental impact oscillator, *Chaos, Solitons & Fractals* 8 (4) (1997) 699–714.
[19] C.J. Begley, L.N. Virgin, Impact response and the influence of fiction, *Journal of Sound and Vibration* 211 (5) (1998) 801–818.
[20] K.N. Slade, L.N. Virgin, P.V. Bayly, Extracting information from interimpact intervals in a mechanical oscillator, *Physical Review E* 56 (3) (1997) 3705–3708.
[21] P.T. Piiroinen, L.N. Virgin, A.R. Champneys, Chaos and period-adding: experimental and numerical verification of the grazing bifurcation, *Journal of Nonlinear Science* 14 (2004) 383–404.
[22] A.F. Filippov, Differential equations with discontinuous right-hand side, *American Mathematical Society Translations* 42 (2) (1968) 199–231.
[23] S. Divenyi, M.A. Savi, L.F.P. Franca, H.I. Weber, Nonlinear dynamics and chaos in systems with discontinuous support, *Shock and Vibration* 13 (4/5) (2006) 315–326.
[24] F. Casas, W. Chin, C. Grebogi, E. Ott, Universal grazing bifurcation in impact oscillators, *Physical Review E* 53 (1996) 134–139.
[25] H.E. Nusse, E. Ott, J.A. Yorke, Border-collision bifurcation: an explanation for observed phenomena, *Physical Review E* 49 (1994) 1073–1076.